RSC Advances

PAPER

View Article Online
View Journal | View Issue

Cite this: *RSC Adv.*, 2023, **13**, 14435

Solvent and catalyst free vitrimeric poly(ionic liquid) electrolytes†

Zviadi Katcharava, [a] Xiaozhuang Zhou, [a] Rajesh Bhandary,[a] Rene Sattler,[b] Heiko Huth,[b] Mario Beiner,[b] Anja Marinow [a] and Wolfgang H. Binder *[a]

Received 11th April 2023
Accepted 28th April 2023

DOI: 10.1039/d3ra02396f

rsc.li/rsc-advances

Polymer electrolytes (PEs) are a promising alternative to overcome shortcomings of conventional lithium ion batteries (LiBs) and make them safer for users. Introduction of self-healing features in PEs additionally leads to prolonged life-time of LIBs, thus tackling cost and environmental issues. We here present solvent free, self-healable, reprocessable, thermally stable, conductive poly(ionic liquid) (PIL) consisting of pyrrolidinium-based repeating units. PEO-functionalized styrene was used as a co-monomer for improving mechanical properties and introducing pendant OH groups in the polymer backbone to act as a transient crosslinking site for boric acid, leading to the formation of dynamic boronic ester bonds, thus forming a vitrimeric material. Dynamic boronic ester linkages allow reprocessing (at 40 °C), reshaping and self-healing ability of PEs. A series of vitrimeric PILs by varying both monomers ratio and lithium salt (LiTFSI) content was synthesized and characterized. The conductivity reached 10^{-5} S cm^{-1} at 50 °C in the optimized composition. Moreover, the PILs rheological properties fit the required melt flow behavior (above 120 °C) for 3D printing *via* fused deposition modeling (FDM), offering the possibility to design batteries with more complex and diverse architectures.

Introduction

Lithium-ion batteries (LiBs) have become increasingly popular in the past two decades and are widely used in a broad range of applications, from consumer electronics to vehicles.[1] One of the key components of a lithium-ion battery is the electrolyte, which is responsible for ion transport between electrodes during charging and discharging. Typically used electrolytes nowadays consist of lithium salts dissolved in organic solvents, which present significant safety concerns due to their flammability.[2,3] Additionally, the mechanical damage of LiBs may lead to a leakage of the liquid electrolyte, thus further increasing fire risk. Different approaches have been developed to overcome these safety concerns.[4,5] Polymer-based electrolytes (PEs) represent an auspicious strategy towards alternative materials for replacing current technologies. PEs exhibit improved safety, higher thermal stability and can hinder formation of Li-dendrites, but all this at the price of reduced performance in terms of ion conductivity.[6,7] However, due to the extreme stress during battery operation PEs may break, leading to a direct contact between electrodes and subsequent short circuit. Thus, introducing self-healing functionality in PE additionally enhances a life-time of LiBs.[8] Furthermore, PEs provide improved mechanical properties and offer the possibility to create batteries with specific shapes and designs suitable for wider range of application. Features of polymeric materials can be tuned in a way to make them suitable for application in additive manufacturing of LiBs. 3D printing of electrolytes and batteries in general can be a useful tool for producing complex structured devices with high precision. Until now mainly successful fabrication of electrode materials *via* additive manufacturing is reported,[9,10] while successful 3D-printing of electrolyte remains a bottleneck of the technology.[11–13]

Due to their unique and favourable properties ionic liquids (ILs) as well as their polymeric analogues – polymeric ionic liquids (PILs) are regarded as promising candidates as electrolytes in next-generation LiBs.[14–17] PILs combine advantageous properties of ILs and polymers: high electrochemical stability, high thermal stability and relatively high conductivity, while simultaneously allowing the introduction of self-healing features into the material. Introducing self-healing abilities in electrolytes proved to extend the cyclic lifetime of the battery.[8,18–20] This can be achieved *via* incorporating dynamic covalent or noncovalent supramolecular bonds/interactions between polymer chains. Noncovalent bonds/interactions are classically hydrogen bonding, ionic interaction, pi–pi stacking *etc.*[8,20,21] Polymers crosslinked *via* dynamic covalent bonds are

[a]*Macromolecular Chemistry, Division of Technical and Macromolecular Chemistry, Faculty of Natural Sciences II (Chemistry, Physics, Mathematics), Institute of Chemistry, Martin Luther University Halle-Wittenberg, von-Danckelmann-Platz 4, D-06120, Halle, Germany. E-mail: wolfgang.binder@chemie.uni-halle.de*

[b]*Fraunhofer Institute for Microstructure of Materials and Systems IMWS, Walter Hülse Str. 1, D-06120, Halle (Saale), Germany*

† Electronic supplementary information (ESI) available: Materials and methods, synthetic procedures and all obtained compositions, NMR, BDS, TGA and WAXD data are presented. See DOI: https://doi.org/10.1039/d3ra02396f

known as vitrimers (also referred as dynamic covalent network (DCN) or covalent adaptable network (CAN) polymers) and represent a relatively new class of materials.[22–24] According to their nature vitrimers are situated between thermosets and thermoplastics, allowing reprocessing or reshaping above threshold temperatures without losing their initial properties. Thus, vitrimers are recyclable, directly addressing the environmental quests related to polymer consumption and usage. Various chemistries were investigated for potential application in vitrimers:[22,25] transesterification,[26–28] transamination,[29,30] disulfide bond exchange,[31–33] silyl ether exchange,[34,35] siloxane exchange,[36] boronic ester exchange[37,38] *etc.*

An only limited number of vitrimeric materials have been developed for potential application as an electrolyte in LiBs. Evans *et al.* reported poly(ethylene oxide)-based vitrimer crosslinked *via* dynamic boronic ester bonds.[39] The conductivity of the material reached 3.5×10^{-4} at 90 °C with an optimized amount of added lithium bis(trifluoromethanesulfonyl)imide (LiTFSI). Furthermore, they demonstrated that crosslinking can be broken down by a solvent and subsequently restored to its original properties. Another PEO based electrolyte with vitrimeric nature was reported by Xue *et al.*,[40] containing disulfide bonds (dynamic covalent crosslinking) as well as hydrogen bonding *via* urea functional groups (supramolecular crosslinking), inducing self-healing even at RT without compromising ion conductivity (reached 2.2×10^{-4} S cm^{-1} at 80 °C) or the cyclic performance. Rowan and co-workers[41] designed different type of PEO-based conductive polymer electrolyte. Wherein dynamic disulfide bridges serve as an adhesion enhancer and also positively impact ion conductivity, reaching 1×10^{-4} S cm^{-1} at 90 °C for an optimized composition (crosslinking density, amount of LiTFSI). An ion conductive, solvent and catalyst-free perfluoropolyether-based vitirimeric material was reported by Ameduri and co-workers[42] with σ ranging between 0.5×10^{-6} and 1.1×10^{-6} S cm^{-1} without additional lithium salt. Drockenmuller *et al.* reported a solvent free PIL vitrimer consisting of poly(1,2,3-triazole)s crosslinked by 1,6 dibromo hexane. Self-healing and reprocessability were achieved *via* a transalkylation exchange of C–N Bonds. However, the observed conductivity values were too low for a practical application as an electrolyte (2×10^{-8} S cm^{-1} at 30 °C). Recently Plesse and co-workers developed a solvent-free ionoelastomer vitrimer consisting of imidazolium-based PIL and PEO copolymer and dynamic boronic ester crosslinker.[43] The material showed exceptional mechanical properties and a conductivity up to 1.6×10^{-5} at 30 °C.

We here report solvent and catalyst-free vitrimeric PIL as potential electrolyte for LiBs. The material combines desired properties such as self-healing, non-flammability, reprocessability, recyclability and ion conductivity. We are using a copolymer containing pyrrolidinium IL-moiety as an ion-conducting part, and EO-containing styrene, whereby EO chains are promoting Li-ion transport and simultaneously enabling a subsequent, transient crosslinking with boric acid to implement vitrimeric behavior. In addition, rheological properties of the vitrimeric PIL meets the requirement for fused deposition modeling (FDM)[44] and 3D structures can be successfully printed. The here reported materials behave like thermoplastics at elevated temperature and after extrusion reform crosslinking or drastically reduce the bond exchange reactions and persist in a printed shape.

Results and discussion

Synthesis of PILs

Synthesis of PILs was achieved *via* free radical copolymerization of two monomers: *N*-[(2-acryloyloxy)propyl]-*N*-methylpyrrolidinium bis(trifluoromethylsulfonyl)amide (**M1**) for introducing unique properties of IL and triethyleneglycol-mono-4-vinylbenzylether (**M2**) as a source of terminal OH

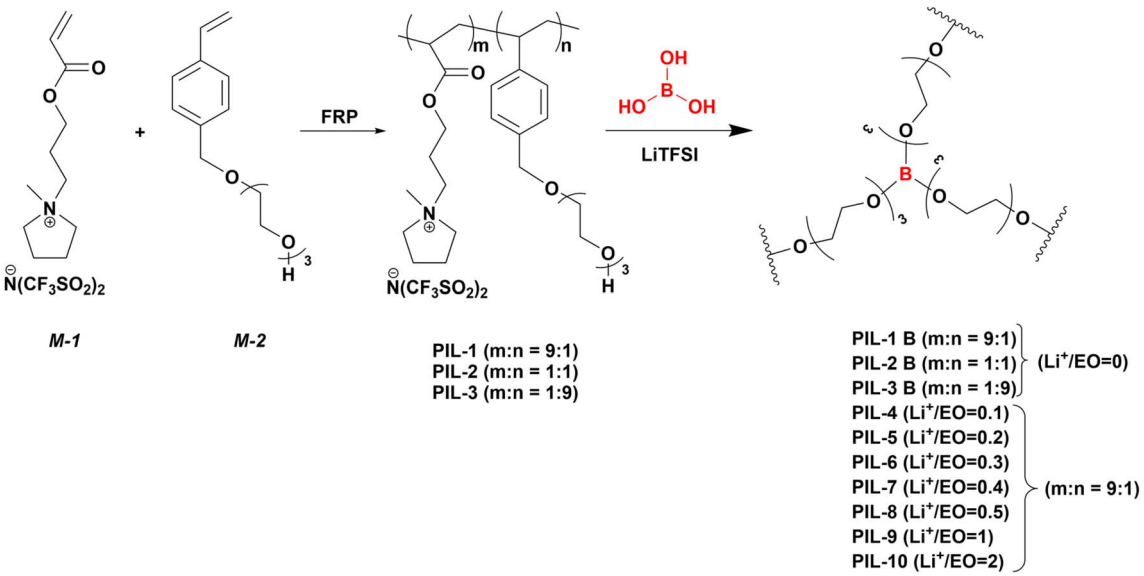

Fig. 1 Synthetic route of PILs and corresponding vitrimers with different content of salt (n(LiTFSI)/n(EO)).

Table 1 Vitrimeric PIL compositions, corresponding monomer ratios (M1/M2), content of LiTFSI and ionic conductivity at 30 °C

Sample	Monomer ratio (M1/M2)[a]	Li^+/EO[a]	Conductivity at 30 °C (S cm^{-1})
PIL-1B	9 : 1	0	1.9×10^{-7}
PIL-2B	1 : 1	0	1.7×10^{-7}
PIL-3B	1 : 9	0	1.5×10^{-7}
PIL-4	9 : 1	0.1	8.8×10^{-7}
PIL-5	9 : 1	0.2	1.7×10^{-6}
PIL-6	9 : 1	0.3	2.5×10^{-6}
PIL-7	9 : 1	0.4	1.6×10^{-6}
PIL-8	9 : 1	0.5	1.2×10^{-6}
PIL-9	9 : 1	1	5.1×10^{-7}
PIL-10	9 : 1	2	4.8×10^{-7}

[a] Molar ratio.

group capable to undergo crosslinking (Fig. 1). We chose pyrrolidinium based IL monomer due to its high electrochemical stability and conductivity.[45–47] Three main compositions with different molar ratios of monomers were prepared, **PIL-1**, **PIL-2**, **PIL-3** with **M1/M2** ratios of 9 : 1, 1 : 1 and 1 : 9, respectively. Obtained molecular weighs were determined using size exclusion chromatography (SEC): **PIL-1** (M_n = 12 kDa, M_w = 94 kDa, PDI = 7.67), **PIL-2** (M_n = 77 kDa, M_w = 225 kDa, PDI = 2.93) and **PIL-3** (M_n = 75 kDa, M_w = 318 kDa, PDI = 4.2). However, it should be mentioned that those values may be imprecise with increasing amount of an IL monomer incorporated in the polymer. Charged ionic liquid moieties are affecting the hydrodynamic radius of polymer chains, leading to altered interactions with the GPC columns. Hence, conventional calibration (with commercial PS or PEO standards) of the SEC is not sufficient to extract accurate data.[48,49] The successful copolymerization and corresponding monomer ratios were verified *via* proton NMR spectroscopy (ESI, S3†). Calculated ratios were in very close proximity to the projected values. After successful polymerization vitrimers were prepared by mixing polymer precursors (**PIL-1**, **PIL-2**, **PIL-3**) with equimolar amount of boric acid for introducing dynamic covalent bonds into the network (**PIL-1B**, **PIL-2B**, **PIL-3B**). **PIL-1** was also mixed with boric acid and different ratios of LiTFSI (with respect to EO amount in the polymer chain) as conductive lithium salt for generating vitrimeric electrolytes. LiTFSI is highly hygroscopic and thus, samples were dried at 120 °C for at least 48 hours for moisture removal. All prepared vitrimeric compositions are listed in the Table 1.

Mechanical characterization

The mechanical properties of an electrolyte can play a crucial role for improving the safety of LiBs. **PIL-1B**, **PIL-2B**, **PIL-3B** were analysed using tensile test at RT in order to choose the optimal composition for further investigations. In Fig. 2A the obtained stress–strain curves as well as the corresponding toughness values are presented. As expected, when we compare the same composition (ratio of **M1/M2**) of PIL before and after crosslinking (**PIL-1** *vs.* **PIL-1B**) we can see that the toughness is significantly increased after crosslinking *via* boronic acid.

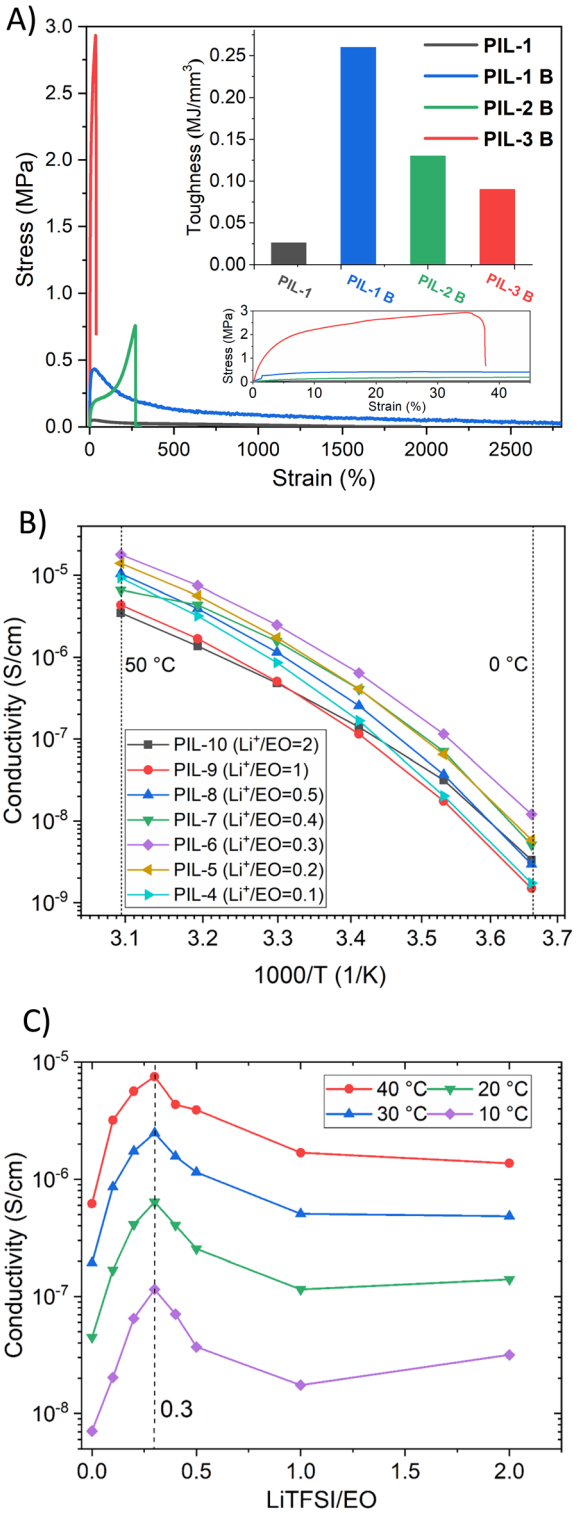

Fig. 2 (A) Tensile measurements with corresponding toughness of PIL-1, PIL-1B, PIL-2B and PIL-3B at RT and zoomed in curve in the strain range of 0–50%; (B) conductivity as a function of temperature for PIL-5–PIL-10; (C) conductivity as a function of lithium content (LiTFSI/EO) at different temperatures.

Furthermore, **PIL-1B** displayed the highest value of toughness (≈0.25 MJ mm^{-3}) compared to **PIL-2B** and **PIL-3B** samples with higher crosslinking density directly related to the higher

content of styrene monomer (**M2**). Although **PIL-2B** and **PIL-3B** can withstand more stress before breaking, they behave more like a brittle material due to restricted dynamics by high degree of crosslinking. The monomer ratio of 9 : 1 (**M1**/**M2**) was used for further sample preparation as it displayed the highest resistance before rupturing.

BDS measurements

Besides good mechanical properties and resolved safety concerns the material should possess good ionic conductivity to be attractive as electrolyte for LiBs. Various vitrimeric samples with different content of LiTFSI (Table 1) were analysed *via* broadband dielectric spectroscopy (BDS). DC conductivities (σ) were extracted from the plateau of frequency *vs.* conductivity plots (ESI, S6†). Fig. 2B shows σ *vs.* T for **PIL-4** to **PIL-10** in the temperature range of 0 to 50 °C. An increase of three orders of magnitude is observed in all compositions with increasing temperature. The highest value was reached for **PIL-6** (1.8×10^{-5} S cm^{-1} at 50 °C). It should be noted that conductivity behaviour reflects Vogel–Tammann–Fulcher (VFT) dependence, which can be the indication that the polymer network exhibits distinct degree of mobility/dynamics despite crosslinking by boronic ester bonds.[50,51] Furthermore, the content of lithium salt significantly impacts the conductivity in polymer electrolyte as it was reported previously.[39,52] Similar trends are also observed here as it can be seen in Fig. 2C. The addition of Li-salt leads to an initial increase of σ, but with the increased content of LiTFSI the conductivity is reducing. Such behaviour was previously reported for PEO-based materials[39,52] but the ratio of LiTFSI/EO is higher in our case presumably due to additional impact of ionic nature of PIL on the coordination environment and interactions between polymer chains and the Li ions compared to pure PEO. In addition, the conductivity trend *vs.* salt content is unchanged, irrespective of the temperature, reaching it maximum when LiTFSI/EO = 0.3 (Fig. 2C).

Thermal properties

Thermogravimetric analysis (TGA) was performed under a nitrogen atmosphere to investigate thermal stability of PIL vitrimers. Initially precursor polymers were analysed. **PIL-2** and **PIL-3** displayed two steps degradation while **PIL-1** showed only one step degradation (ESI, S4†). Fig. 3A shows TGA curves of vitrimeric compositions. An insignificant weight loss (less than 5 wt%) of PILs is observed till 300 °C for all samples. The degradation follows the same path irrespectively to the salt content or degree of crosslinking in the sample.

Thermal transitions were investigated by different scanning calorimetry (DSC) (Fig. 3B). A glass transition (T_g) which is related to segmental motions, was observed in the range between 7 °C to −12 °C. The addition of LiTFSI is not changing the nature of the samples, since a distinct T_g is still observed. The T_g displays gradual decrease with increasing content of LiTFSI, which is in accordance with previously reported PIL-based polymers/lithium salt compositions.[53–55] As expected the reduction of T_g impacts the conductivity and the composition with Li$^+$/EO = 2.0 (**PIL-10**) displayed higher conductivity

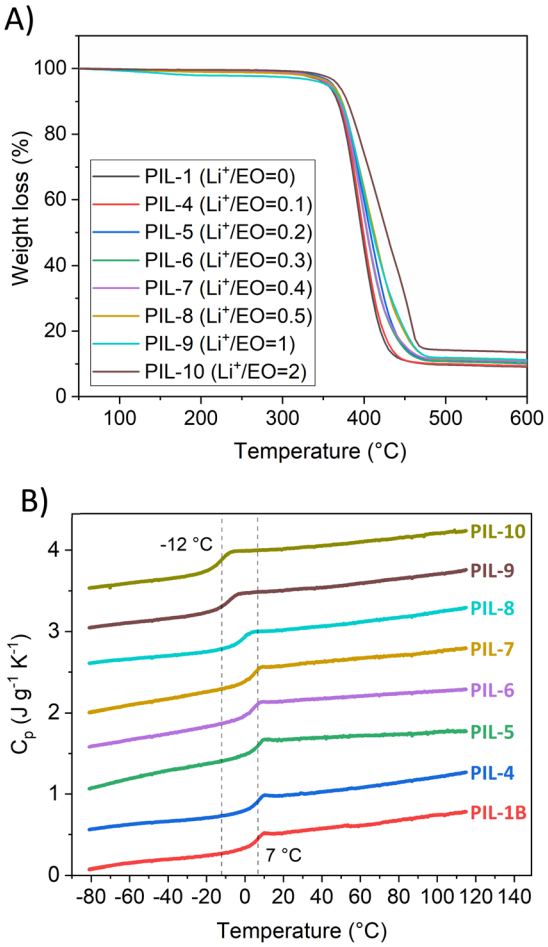

Fig. 3 (A) TGA curves of vitrimeric compositions, measured under N_2 in the temperature range from 35 °C to 600 °C; (B) DSC analysis of PIL compositions from −80 °C to 120 °C with the heating rate of 5 K min.

compared to ratio 1.0 (**PIL-9**) at lower temperatures. The deviation from the trend can be due to higher chain mobility in **PIL-10**. Furthermore, vitrimeric PILs displayed typical amorphous behaviour with no crystallization or melting peaks.

Rheological properties

Dynamic networks are commonly characterized by rheological measurements. Most importantly, stress relaxation experiments can be used to determine the activation energy (E_a) and topology freezing temperature (vitrimer transition temperature, T_v). T_v indicates the temperature above which dynamic bond exchange rate is significant and the polymer network can undergo topology rearrangement.[56,57] Fig. 4A and B show normalized stress–relaxation curves at different temperatures of **PIL-1B** and **PIL-4**. These two samples were chosen to investigate the influence of additional LiTFSI on the relaxation behaviour. According to the Maxwell model for viscoelastic fluids the relaxation time is determined as the time when the normalized stress value reaches $1/e$.[29,58,59] By plotting the $1/e$ times for each temperature we can observe Arrhenius behaviour (Fig. 4C and D). The fittings follow the equation: $\ln(\tau^*) = \ln(\tau_0) + E_a/RT$,

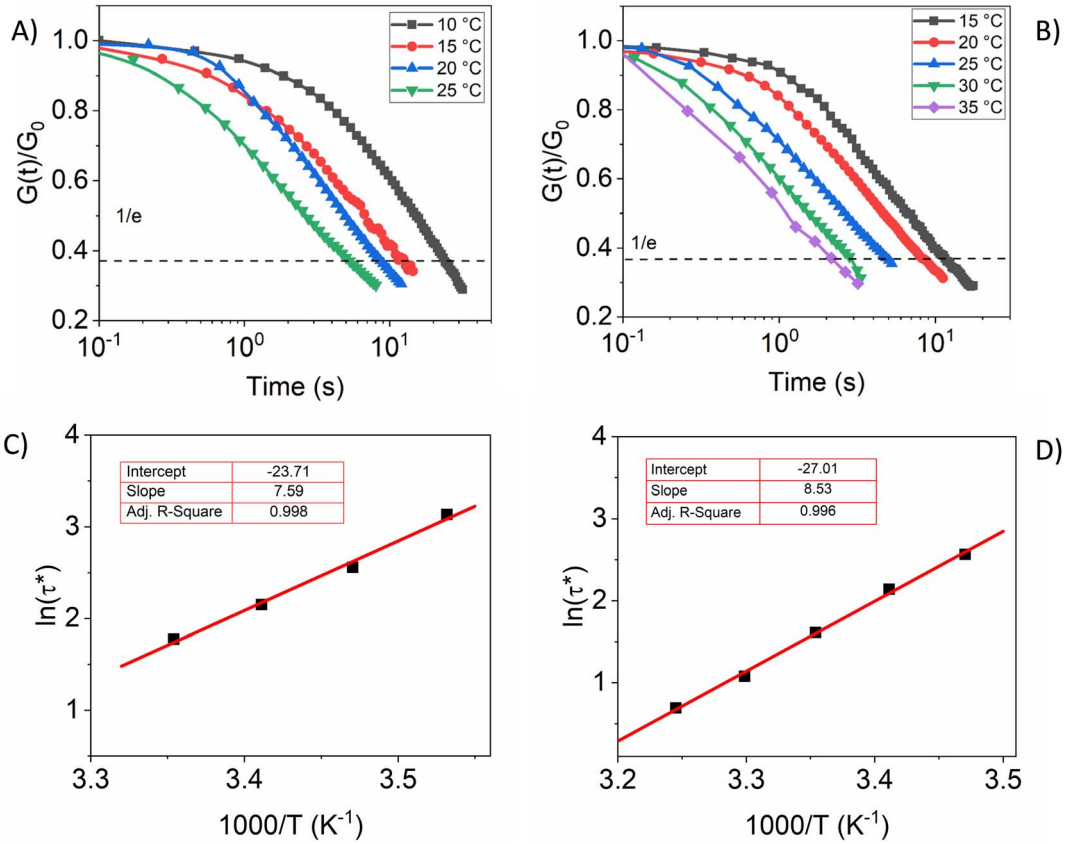

Fig. 4 Stress relaxation curves of (A) **PIL-1B**, (B) **PIL-4**; relaxation times as a function of inverse temperature and Arrhenius fitting for (C) **PIL-1B**, (D) **PIL-4**.

where τ_0 is the characteristic relaxation time, E_a is the activation energy, and R is the universal gas constant. E_a can be calculated form the slope of the Arrhenius equation which is 61.7 kJ mol^{-1} for **PIL-1B** (Fig. 4C) and 70.9 kJ mol^{-1} for **PIL-4** (Fig. 4D). The values are in the similar range as observed for other boronic ester based vitrimers reported before.[38,60]

Viscoelastic behaviour of vitrimers is characterized mainly by two transition temperatures: the glass transition and the topology freezing temperature. Traditionally T_v corresponds to the temperature when the viscosity of materials reaches 10^{12} Pa s. Due to the difficulty to measure viscosities at this high range, a few alternative methods have been developed to determine transition temperature (including stress relaxation measurements).[25,56,57,61,62] The Maxwell relation can be applied to approximate T_v,[23] the temperature when the relaxation time is in the order of 10^6 s. By extrapolating the Arrhenius fit in Fig. 4C and D (temperature at ln(10^6)) we calculated T_v (**PIL-1B**) = −71 °C and T_v (**PIL-4**) = −64 °C, respectively. However, the values obtained by extrapolation can have a high inaccuracy[63] especially in this case as the Arrhenius behaviour could be approaching nonlinear WLF behaviour close to T_g.[34] In addition we can see that the difference between two samples is insignificant in terms of E_a and T_v. Presumably the addition of LiTFSI is not drastically changing the interaction environment of materials, thus polymer dynamics persist unchanged. Wide angle X-ray diffraction (WAXD) measurements additionally proved that there are no structural changes after the addition of lithium salt to PILs (ESI, S8†)

Self-healing/reprocessing

The presence of dynamic covalent bonds introduces self-healing ability to the PILs, which can be characterized by tensile tests before and after self-healing. **PIL-1B** was hot-vacuum-pressed to prepare a rectangular shape specimen, which was later cut into two pieces and kept together in the oven at 80 °C for 30 min (Fig. 5A). Successful self-healing could be visually observed and quantified *via* tensile testing. After self-healing the toughness of **PIL-1B** could be restored to 65% of its original state (Fig. 5A). It should be highlighted that no pressure was applied during the self-healing process. This might result in imperfect adhesion between cut pieces, which can later induce crack propagation (hence reduce toughness). Nevertheless, the self-healing of these PILs is effective and can restore properties in a short period of time. Furthermore, PILs can be reprocessed using hot vacuum pressing. **PIL-1B** was cut into small pieces and placed in a hot-vacuum-press (Fig. 5B) at 40 °C for 4 hours. It can be seen that the integrity of samples was fully restored. In addition, PILs were probed for 3D printing *via* fused deposition modelling. FDM was performed at 120 °C where the bond exchange rate is high and the material exhibits suitable viscosity for extrusion. Fig. 5C shows 3D printed **PIL-5** into star shape,

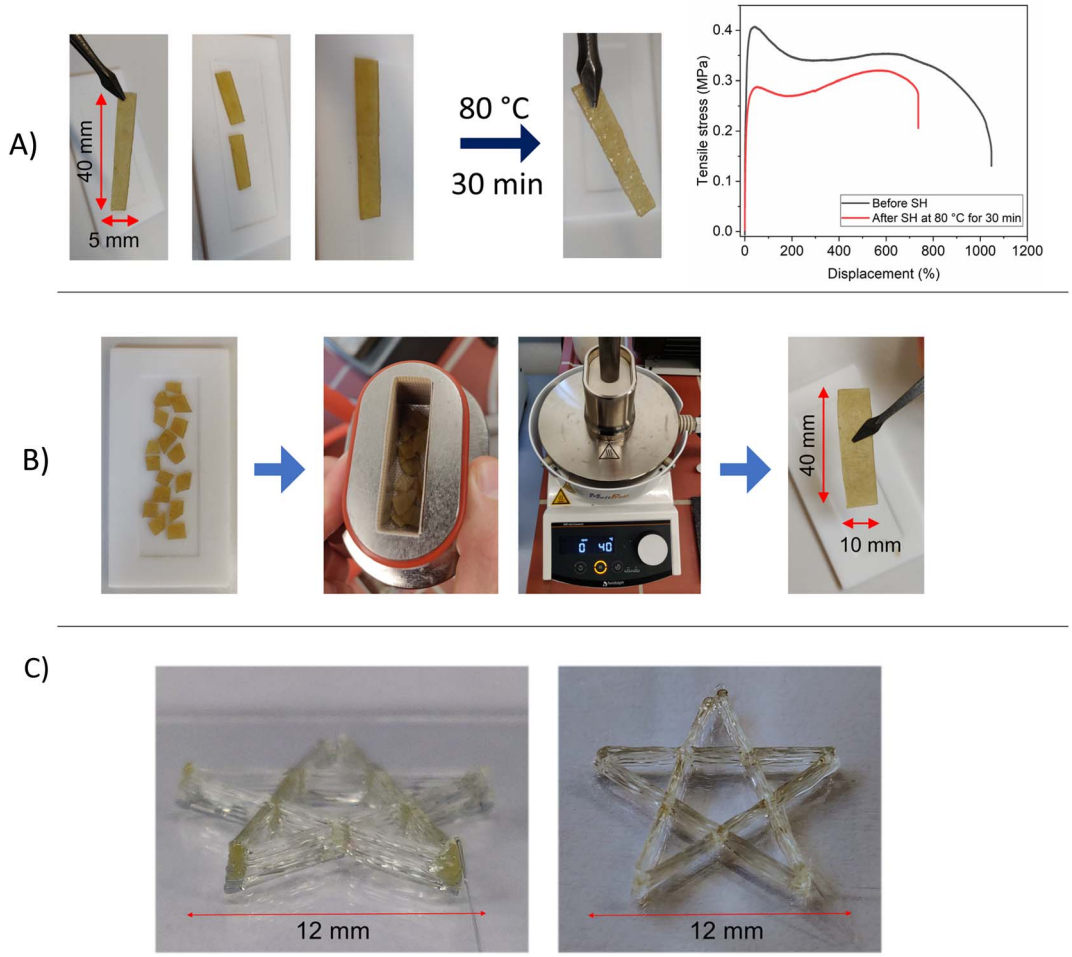

Fig. 5 (A) self-healing experiment of **PIL1-B** and corresponding tensile test; (B) reprocessing of **PIL-1B** *via* hot press; (C) FDM of **PIL-5** into star shape.

where 7 consecutive layers were printed directly on the glass plate (in normal laboratory conditions). The printed shape showed good stability in water free environment, proving the possible application of PILs in additive manufacturing of batteries.

Conclusions

Pyrrolidinium based vitrimers were successfully prepared with different ratios of ionic liquid and styrene-EO based monomers and boric acid as crosslinker. Monomer ratio (crosslinking density) can be used as a tool to adjust the materials mechanical property according to application requirements. The composition (**M1**/**M2** = 9/1) displaying the highest toughness was used for further investigation. PILs displayed good conductivity (up to 1.8×10^{-5} S cm^{-1} at 50 °C) for optimal content of lithium salt (Li^+/EO = 0.3) and a high thermal stability (up to 300 °C) for all compositions. Furthermore, boronic ester bonds allowed the material to be self-healable, reprocessable and applicable for FDM. Successful 3D printing *via* FDM was performed at 120 °C and showed good adhesion between extruded layers. Vitrimeric PILs showed promising properties to be used as electrolyte for current and future LiBs technologies.

Experimental

Synthetic procedures

Synthesis of M1 and M2. Monomers were synthesised in multiple step process and the purity was verified by NMR spectroscopy. Monomers were dried *via* high vacuum pump over P_2O_5 for removing traces of moisture. Detailed procedures are given in the ESI.†

Synthesis of PIL-1, PIL-2, PIL-3. In a typical polymerization of **PIL-1** – 4 g (8.37 mmol) **M1**, 0.234 g (0.93 mmol) **M2** and 0.021 g AIBN were dissolved in dry DMF (4 mL). After freeze thaw cycles (3×) the mixture was placed in an oil bath at 70 °C overnight (under inert atmosphere). The reaction product was precipitated into DCM. A highly viscous polymer was collected *via* decantation, dissolved in 5 mL acetone and precipitated again in DCM. Previous precipitation steps were repeated 3 times. Finally, the polymer was dried in a vacuum oven at 65 °C for 18 hours.

Similarly, **PIL-2** and **PIL-3** were synthesised with different ratios of monomers. DCM/hexane with volume ratios of 1/1 were used for precipitation step.

Synthesis of vitrimeric PILs. In a typical procedure 1.5 g PIL-1 was dissolved in 5 mL dry acetonitrile. Dry LiTFSI dissolved in

1 mL ACN was added to the polymer solution. Boric acid was dissolved in methanol (stock solution) and an appropriate amount was added to the mixture (exact amount for each composition is given in the ESI). The solution was kept stirring at 40 °C for 30 min. The temperature was gradually increased to 100 °C while the flask was under a constant flow of nitrogen for letting the ACN evaporate. A highly viscous product was transferred to a Teflon mold and dried in vacuum oven at 120 °C for 48 hours at least.

Methods

Conductivity measurements

A Broadband Dielectric Spectroscopy (BDS) Novocontrol "Alpha analyzer" was used for investigating ionic conductivities. Samples were placed in a cell containing two brass electrodes (d = 20 mm, h = 2.5 mm), applied small pressure on cell for ensuring proper contact between electrodes and samples. Measuring cell placed in a cryostat with a constant flow of dry nitrogen. Ionic conductivity was recorded in the frequency range 1–10^6 Hz and different temperatures. Values were extracted from the plateau of σ *vs.* T.

Thermogravimetric analysis (TGA)

TGA was conducted on Netzsch TG 209 F3. Polymer samples (5–10 mg) were placed in alumina crucibles and heated from 35 °C to 800 °C with the heating rate of 10 K min^{-1} under nitrogen atmosphere (flow rate 20 mL min^{-1}). The NETZSCH Proteus was used for analysing recorded data.

Differential scanning calorimetry (DSC)

DSC data were collected using a PerkinElmer Pyris7. Thermal history was removed by heating up to 120 °C and holding the respective sample at 120 °C for 30 min. The samples were subsequently cooled to −80 °C with a cooling rate of 5 K min^{-1}. Heating curves were recorded form −80 °C to 120 °C (heating rate 5 K min^{-1}). Temperature calibration was performed manually using OriginLab2023. Substances for temperature calibration were water, indium, tin and lead.

Rheology

Anton Paar MCR-101 DSO rheometer equipped with parallel plate–plate geometry (d = 8 mm) was used for rheology measurements. Device was equipped with Peltier-temperature control for ensuring accurate temperature control and nitrogen gas flushing. All samples were pre dried at 120 °C for 24 hours. Recorded data was analysed *via* RheoCompass™.

3D printing

3D printing was performed on RegenHU 3D Discovery equipped with a storage tank (heatable) and an extrusion printing head. A needle with the size of 0.33 mm was connected to the printing head and a pressure of 0.2 MPa was applied for generating a constant flow of PIL through the nozzle. 120 °C was chosen (for the nozzle and storage tank) for FDM. BioCAD™ program was used for designing shapes for printing. FMD was performed by directly on glass surfaces in normal laboratory conditions.

Author contributions

Conceptualization, W. H. B., X. Z. and Z. K.; data curation, Z. K. and X. Z.; formal analysis, Z. K., X. Z., R. S. and R. B.; funding acquisition, W. H. B. and A. M.; investigation, Z. K. and X. Z.; methodology, Z. K., W. H. B. and X. Z.; project administration, A. M. and W. H. B.; resources, W. H. B.; software, Z. K. and H. H.; supervision, W. H. B.; validation, Z. K., R. B., A. M., X. Z. and W. H. B.; visualization, Z. K.; writing—original draft preparation, Z. K. and A.M.; writing—review and editing, Z. K., A. M., R. B., X. Z., R. S., M. B. and W. H. B.; All authors have read and agreed to the published version of the manuscript.

Conflicts of interest

There are no conflicts to declare.

Acknowledgements

This research was developed under the framework of the BAT4EVER project. This project has received funding from the European Union's Horizon 2020 research and innovation programme under grant agreement no 957225. The financial support by the DFG project BI 1337/14-1 is gratefully acknowledged. The authors are grateful to Dr Boyan Iliev and IoLiTec Ionic Liquids Technologies GmbH for fruitful discussions.

References

1 M. Li, J. Lu, Z. Chen and K. Amine, *Adv. Mater.*, 2018, **30**, 1800561.
2 K. Liu, Y. Liu, D. Lin, A. Pei and Y. Cui, *Sci. Adv.*, 2018, **4**, eaas9820.
3 Q. S. Wang, L. H. Jiang, Y. Yu and J. H. Sun, *Nano Energy*, 2019, **55**, 93–114.
4 K. Xu, *Chem. Rev.*, 2014, **114**, 11503–11618.
5 D. Zhou, D. Shanmukaraj, A. Tkacheva, M. Armand and G. X. Wang, *Chem*, 2019, **5**, 2326–2352.
6 Y. An, X. Han, Y. Liu, A. Azhar, J. Na, A. K. Nanjundan, S. Wang, J. Yu and Y. Yamauchi, *Small*, 2022, **18**, e2103617.
7 V. Vijayakumar, M. Ghosh, P. K. Samantaray, S. Kurungot, M. Winter and J. R. Nair, in *Two-dimensional Inorganic Nanomaterials for Conductive Polymer Nanocomposites*, ed. C. Wan, X. Huang and C. Bowen, The Royal Society of Chemistry, 2021, pp. 204–274, DOI: 10.1039/9781839162596-00204.
8 A. Marinow, Z. Katcharava and W. H. Binder, *Polymers*, 2023, **15**, 1145.
9 M. Pei, H. Shi, F. Yao, S. Liang, Z. Xu, X. Pei, S. Wang and Y. Hu, *J. Mater. Chem. A*, 2021, **9**, 25237–25257.
10 L. Zeng, P. Li, Y. Yao, B. Niu, S. Niu and B. Xu, *Mater. Today Nano*, 2020, **12**, 100094.
11 A. Vlad, N. Singh, C. Galande and P. M. Ajayan, *Adv. Energy Mater.*, 2015, **5**, 1402115.

12 M. Cheng, Y. Jiang, W. Yao, Y. Yuan, R. Deivanayagam, T. Foroozan, Z. Huang, B. Song, R. Rojaee, T. Shokuhfar, Y. Pan, J. Lu and R. Shahbazian-Yassar, *Adv. Mater.*, 2018, **30**, e1800615.
13 Z. Katcharava, A. Marinow, R. Bhandary and W. H. Binder, *Nanomaterials*, 2022, **12**, 1859.
14 M. Armand, F. Endres, D. R. MacFarlane, H. Ohno and B. Scrosati, *Nat. Mater.*, 2009, **8**, 621–629.
15 M. Watanabe, M. L. Thomas, S. Zhang, K. Ueno, T. Yasuda and K. Dokko, *Chem. Rev.*, 2017, **117**, 7190–7239.
16 J. Y. Yuan, D. Mecerreyes and M. Antonietti, *Prog. Polym. Sci.*, 2013, **38**, 1009–1036.
17 W. Qian, J. Texter and F. Yan, *Chem. Soc. Rev.*, 2017, **46**, 1124–1159.
18 W. Mai, Q. Yu, C. Han, F. Kang and B. Li, *Adv. Funct. Mater.*, 2020, **30**, 1909912.
19 E. R. Ezeigwe, L. Dong, R. Manjunatha, M. Tan, W. Yan and J. J. Zhang, *Nano Energy*, 2021, **84**, 105907.
20 J. H. Xu, C. D. Ding, P. Chen, L. H. Tan, C. B. Chen and J. J. Fu, *Appl. Phys. Rev.*, 2020, **7**, 031308.
21 A. Campanella, D. Dohler and W. H. Binder, *Macromol. Rapid Commun.*, 2018, **39**, e1700739.
22 J. Zheng, Z. M. Png, S. H. Ng, G. X. Tham, E. Ye, S. S. Goh, X. J. Loh and Z. Li, *Mater. Today*, 2021, **51**, 586–625.
23 J. C. Luo, Z. Demchuk, X. Zhao, T. Saito, M. Tian, A. P. Sokolov and P. F. Cao, *Matter*, 2022, **5**, 1391–1422.
24 W. Denissen, J. M. Winne and F. E. Du Prez, *Chem. Sci.*, 2016, **7**, 30–38.
25 B. Krishnakumar, R. V. S. P. Sanka, W. H. Binder, V. Parthasarthy, S. Rana and N. Karak, *J. Chem. Eng.*, 2020, **385**, 123820.
26 J. P. Brutman, P. A. Delgado and M. A. Hillmyer, *ACS Macro Lett.*, 2014, **3**, 607–610.
27 Z. Pei, Y. Yang, Q. Chen, E. M. Terentjev, Y. Wei and Y. Ji, *Nat. Mater.*, 2014, **13**, 36–41.
28 M. Capelot, D. Montarnal, F. Tournilhac and L. Leibler, *J. Am. Chem. Soc.*, 2012, **134**, 7664–7667.
29 W. Denissen, G. Rivero, R. Nicolay, L. Leibler, J. M. Winne and F. E. Du Prez, *Adv. Funct. Mater.*, 2015, **25**, 2451–2457.
30 A. Chao and D. H. Zhang, *Macromolecules*, 2019, **52**, 495–503.
31 M. Chen, L. Zhou, Y. Wu, X. Zhao and Y. Zhang, *ACS Macro Lett.*, 2019, **8**, 255–260.
32 A. Ruiz de Luzuriaga, R. Martin, N. Markaide, A. Rekondo, G. Cabañero, J. Rodríguez and I. Odriozola, *Mater. Horiz.*, 2016, **3**, 241–247.
33 M. Pepels, I. Filot, B. Klumperman and H. Goossens, *Polym. Chem.*, 2013, **4**, 4955–4965.
34 Y. Nishimura, J. Chung, H. Muradyan and Z. Guan, *J. Am. Chem. Soc.*, 2017, **139**, 14881–14884.
35 S. W. Wu, Z. J. Yang, S. F. Fang, Z. H. Tang, F. Liu and B. C. Guo, *J. Mater. Chem. A*, 2019, **7**, 1459–1467.
36 P. Zheng and T. J. McCarthy, *J. Am. Chem. Soc.*, 2012, **134**, 2024–2027.
37 O. R. Cromwell, J. Chung and Z. Guan, *J. Am. Chem. Soc.*, 2015, **137**, 6492–6495.
38 M. Rottger, T. Domenech, R. van der Weegen, A. Breuillac, R. Nicolay and L. Leibler, *Science*, 2017, **356**, 62–65.
39 B. B. Jing and C. M. Evans, *J. Am. Chem. Soc.*, 2019, **141**, 18932–18937.
40 Y. H. Jo, S. Li, C. Zuo, Y. Zhang, H. Gan, S. Li, L. Yu, D. He, X. Xie and Z. Xue, *Macromolecules*, 2020, **53**, 1024–1032.
41 R. Kato, P. Mirmira, A. Sookezian, G. L. Grocke, S. N. Patel and S. J. Rowan, *ACS Macro Lett.*, 2020, **9**, 500–506.
42 G. Lopez, L. Granado, G. Coqui, A. Larez-Sosa, N. Louvain and B. Ameduri, *Macromolecules*, 2019, **52**, 2148–2155.
43 F. Li, G. T. M. Nguyen, C. Vancaeyzeele, F. Vidal and C. Plesse, *ACS Appl. Polym. Mater.*, 2023, **5**, 529–541.
44 H. Rupp and W. H. Binder, *Front. Chem.*, 2021, **9**, 771974.
45 D. R. MacFarlane, P. Meakin, J. Sun, N. Amini and M. Forsyth, *J. Phys. Chem. B*, 1999, **103**, 4164–4170.
46 M. Hayyan, F. S. Mjalli, M. A. Hashim, I. M. AlNashef and T. X. Mei, *J. Ind. Eng. Chem.*, 2013, **19**, 106–112.
47 A. Lewandowski and A. Swiderska-Mocek, *J. Power Sources*, 2009, **194**, 601–609.
48 C. Li, R. Bhandary, A. Marinow, D. Ivanov, M. Du, R. Androsch and W. H. Binder, *Polymers*, 2022, **14**, 4090.
49 H. He, M. Zhong, B. Adzima, D. Luebke, H. Nulwala and K. Matyjaszewski, *J. Am. Chem. Soc.*, 2013, **135**, 4227–4230.
50 K. M. Diederichsen, H. G. Buss and B. D. McCloskey, *Macromolecules*, 2017, **50**, 3832–3841.
51 F. Baskoro, H. Q. Wong and H. J. Yen, *ACS Appl. Energy Mater.*, 2019, **2**, 3937–3971.
52 M. Chintapalli, T. N. P. Le, N. R. Venkatesan, N. G. Mackay, A. A. Rojas, J. L. Thelen, X. C. Chen, D. Devaux and N. P. Balsara, *Macromolecules*, 2016, **49**, 1770–1780.
53 A. Yokokoji, W. Kitayama, K. Wichai, O. Urakawa, A. Matsumoto, V. Vao-Soongnern and T. Inoue, *Polymers*, 2021, **13**, 1772.
54 X. Wang, F. Chen, G. M. A. Girard, H. Zhu, D. R. MacFarlane, D. Mecerreyes, M. Armand, P. C. Howlett and M. Forsyth, *Joule*, 2019, **3**, 2687–2702.
55 R. Löwe, T. Hanemann, T. Zinkevich and A. Hofmann, *Polymers*, 2021, **13**, 792.
56 M. Capelot, M. M. Unterlass, F. Tournilhac and L. Leibler, *ACS Macro Lett.*, 2012, **1**, 789–792.
57 H. Fang, W. Ye, Y. Ding and H. H. Winter, *Macromolecules*, 2020, **53**, 4855–4862.
58 S. Dhers, G. Vantomme and L. Averous, *Green Chem.*, 2019, **21**, 1596–1601.
59 L. E. Porath and C. M. Evans, *Macromolecules*, 2021, **54**, 4782–4791.
60 W. A. Ogden and Z. Guan, *J. Am. Chem. Soc.*, 2018, **140**, 6217–6220.
61 A. M. Hubbard, Y. Ren, D. Konkolewicz, A. Sarvestani, C. R. Picu, G. S. Kedziora, A. Roy, V. Varshney and D. Nepal, *ACS Appl. Polym. Mater.*, 2021, **3**, 1756–1766.
62 Y. Yang, S. Zhang, X. Zhang, L. Gao, Y. Wei and Y. Ji, *Nat. Commun.*, 2019, **10**, 3165.
63 M. Guerre, C. Taplan, J. M. Winne and F. E. Du Prez, *Chem. Sci.*, 2020, **11**, 4855–4870.